The Astrophysical Journal, 625:L59–L62, 2005 May 20

AN ASSESSMENT OF THE Fe XVIII AND Fe XIX LINE RATIOS FROM THE *CHANDRA* GRATING OBSERVATIONS OF CAPELLA

P. Desai,[1] N. S. Brickhouse,[1] J. J. Drake,[1] A. K. Dupree,[1] R. J. Edgar,[1] R. Hoogerwerf,[1] V. Kashyap,[1] B. J. Wargelin,[1] R. K. Smith,[2] D. P. Huenemoerder,[3] and D. A. Liedahl[4]
Received 2005 March 4; accepted 2005 April 12; published 2005 May 3

ABSTRACT

Observations of Fe XVIII and Fe XIX X-ray, extreme-UV, and far-UV line emission, formed at the peak of Capella's (α Aurigae's) emission measure distribution and ubiquitous in spectra of many cool stars and galaxies, provide a unique opportunity to test the robustness of Fe XVIII and Fe XIX spectral models. The Astrophysical Plasma Emission Code (APEC) is used to identify over 35 lines from these two ions alone, and to compare model predictions with spectra obtained with the *Chandra* Low Energy Transmission Grating and High Energy Transmission Grating Spectrometers, the *Far Ultraviolet Spectroscopic Explorer* (*FUSE*), and the *Extreme Ultraviolet Explorer*. Some flux discrepancies larger than a factor of 2 are found between observations of Fe XVIII and Fe XIX lines and predictions by APEC and other models in common use. In particular, the X-ray resonance lines for both ions are stronger than predicted by all models relative to the EUV resonance lines. The multi-wavelength observations demonstrate the importance of including dielectronic recombination and proton-impact excitation, and of using accurate wavelengths in spectral codes. These ions provide important diagnostic tools for 10^7 K plasmas currently observed with *Chandra*, *XMM-Newton*, and *FUSE*.

Subject headings: atomic data — atomic processes — stars: individual (Capella) — ultraviolet: stars — X-rays: stars

1. INTRODUCTION

The Capella system (=HD 34029, α Aurigae), consisting principally of two cool giant stars (G8 III + G1 III), is one of the strongest coronal X-ray sources, and it offers an opportunity to benchmark the models used in the interpretation of X-ray spectra from astrophysical plasmas. Although plasma codes have gone through major improvements (e.g., Mewe et al. 1995; Brickhouse et al. 1995; Smith et al. 2001; Young et al. 2003), their accuracy and completeness for diagnostic analysis at high spectral resolution has yet to be fully assessed. This Letter compares current spectral models for Fe XVIII and Fe XIX with *Chandra* Emission Line Project (ELP) observations of Capella (Brickhouse & Drake 2000) as a step toward ensuring that astrophysical interpretations of spectra are based on a sound understanding of the physical processes involved. The Capella spectrum is well studied, showing no evidence of flares (Brinkman et al. 2001; Canizares et al. 2000). The emission measure distribution (EMD) of the Capella system shows a strong narrow peak at 6 MK, near the temperature of peak emissivity for Fe XVIII and Fe XIX, producing numerous strong transitions. Modest variability (∼20%) of line fluxes from these ions over timescales of months to years (A. K. Dupree et al. 2005, in preparation) validates the combined analysis of multiple observations.

Although Fe L-shell X-ray lines offer powerful diagnostic potential for collisionally ionized plasmas, new discrepancies between models and observations are now arising from *Chandra* spectra. For example, Xu et al. (2002) find that the observed Fe XVIII $3s$–$2p$/$3d$–$2p$ ratio in the elliptical galaxy NGC 4636 is higher than predicted by APEC and similar to the ratio observed in Capella. The analogous Fe XVII ratio shows the same pattern of discrepancy in solar observations (see Saba et al. 1999), suggesting a common atomic physics origin. Laboratory programs (Brown et al. 1998; Laming et al. 2000; Beiersdorfer et al. 2002) have only recently addressed Fe XVII modeling issues. The ELP observations of Capella offer a unique opportunity to compare models and observations over a broad spectral range. Comparisons among far-ultraviolet (FUV), extreme-ultraviolet (EUV), and X-ray lines of Fe XVIII and Fe XIX are particularly useful, since the strong $n = 2 \rightarrow 2$ EUV lines are essentially entirely produced by direct collisional excitation and thus should be easier to interpret than FUV or X-ray lines, which can include contributions from other processes, such as proton-impact excitation and dielectronic recombination (DR).

2. DATA ANALYSIS

2.1. *Observations and Data Reduction*

Multiple spectra of Capella, acquired between 1999 August and 2002 October, include pointings with the *Chandra* High Energy Transmission Grating (HETG) with the ACIS-S detector for a total exposure time of 182.2 ks, and with the Low Energy Transmission Grating (LETG) and HRC-S detector for a total exposure time of 234.2 ks. The HETG and LETG data, obtained from the *Chandra* archive, were reprocessed using CIAO version 3.0[5] with only minor deviations from the standard pipeline procedures. Effective areas were generated for each data set using the *Chandra* calibration database CALDB 2.8 and were exposure-time weighted to create average effective areas for the summed spectra.

Extreme Ultraviolet Explorer (*EUVE*) spectra obtained in 1999 September, which are nearly simultaneous with a *Chandra* LETG/HRC-S pointing, were processed using standard

[1] Harvard-Smithsonian Center for Astrophysics, 60 Garden Street, Cambridge, MA 02138; pdesai@cfa.harvard.edu.

[2] X-Ray Astrophysics Laboratory, Code 662, NASA Goddard Space Flight Center, Greenbelt, MD 20771; and Department of Physics and Astronomy, Johns Hopkins University.

[3] MIT Center for Space Research, 70 Vassar Street, Cambridge, MA 02139.

[4] Lawrence Livermore National Laboratory, L-41, P.O. Box 808, Livermore, CA 94551.

[5] See http://cxc.harvard.edu/ciao.

EUVE Guest Observer software (IRAF). The agreement between LETG and *EUVE* fluxes for the lines discussed in this Letter is good to within about 5%, and henceforth LETG fluxes will be used. The *Far Ultraviolet Spectroscopic Explorer* (*FUSE*) line fluxes are taken from the spectra of Young et al. (2001).

We use the Astrophysical Plasma Emission Code version 1.3 (APEC; Smith et al. 2001) to predict the Capella spectrum.[6] The APEC models for Fe XVIII and Fe XIX contain 501 and 994 fine-structure levels, respectively, up to principal quantum number $n = 5$. They include the effective collision strengths and atomic transition probabilities calculated using the Hebrew University Lawrence Livermore Atomic Code (HULLAC; Liedahl et al. 1995). For Fe XVIII, the collision strengths for the $2p^5\,{}^2P_{1/2}$–$2p^5\,{}^2P_{3/2}$ transition include resonance excitation from ***R***-matrix calculations (Berrington et al. 1998). Proton-impact excitation rates within the ground state are included for Fe XVIII (Foster et al. 1994) and Fe XIX (R. Reid 1999, private communication). Laboratory X-ray wavelengths (Brown et al. 2002) have been incorporated. APEC currently includes DR rates to excited levels of Fe XVII and H- and He-like ions, but not for the other Fe L-shell ions. Similarly, DR satellite lines are present in APEC for Fe XVII (Safronova et al 2001), but not for Fe XVIII and Fe XIX.

2.2. *Spectral Models and Measurements*

We calculate the global continuum spectra produced by bremsstrahlung, radiative recombination continuum, and two-photon emission over the observed *Chandra* spectral range. We then fit the temperature of the continuum model to the line-free regions of the HETG spectrum, identified both from the APEC line list and by visual inspection, which yields a temperature of 6 MK, near the peak of the EMD. Since the LETG spectrum is contaminated by high-order emission, the same continuum model derived from the HETG data is also applied to the LETG fitting. We adopted the abundances of Brickhouse et al. (2000), who found no evidence for deviation from the solar abundances of Anders & Grevesse (1989). Individual line fluxes from the *Chandra* spectra were measured using Sherpa (Freeman et al. 2001) to fit functions approximating the instrumental line profiles. Plus and minus orders were fitted separately, with the requirement that the line fluxes be the same. A narrow range for the FWHM was allowed (for HETG, 0.01–0.0135 Å, and for LETG, 0.045–0.06 Å), standard binning was maintained, and the Cash statistic was applied (Cash 1979). Table 1 gives the observed fluxes for the Fe XVIII and Fe XIX lines with 1 σ errors.

2.3. *Model Assumptions*

A continuous EMD (Brickhouse et al. 2000), composed of eight temperature components on a 0.1 dex grid, is used to estimate the contribution of line blends from ions over the entire temperature range. This EMD is normalized to the flux of the Fe XVIII λ93.92 resonance line and used to predict the line fluxes given in Table 1. We note that there is only a few-percent difference between the single-temperature 6 MK model and the EMD for the lines of interest. Since some Fe XIX line emissivities show modest density sensitivity between the low-density limit and densities expected under coronal conditions, we have used the APEC code to compute models for a wide range of densities. The most affected line ratio is that of λ101.55 to λ108.37. At $N_e = 10^{10}$ cm^{-3} the predicted ratio is 0.347 (in photon units), compared with 0.261 at the standard APEC low-density limit, in better agreement with the observed flux ratio of 0.328.

Lack of significant variability further supports the assumption that the plasma conditions are stable, as individual lines of Fe XVII, Fe XVIII, and Fe XIX show modest flux changes (<10% deviation from the average value) between *Chandra* pointings, and the light curves show low levels of variability (≲8%) during a single pointing. There is also no evidence to challenge the standard assumptions of negligible optical depth (Canizares et al. 2000; Brown et al. 1998).

3. RESULTS AND DISCUSSION

Figure 1 compares the observed Fe XVIII and Fe XIX line fluxes with those predicted by the spectral codes, APEC, CHIANTI version 4.2 (Dere et al. 1997; Young et al. 2003), and SPEX version 1.1 (Kaastra et al. 1996), which incorporates the MEKAL model (Mewe et al 1995). Emissivities provided by M.-F. Gu (2004, private communication) using the Flexible Atomic Code (FAC; Gu 2003) are also compared. The fluxes are scaled by the fluxes of their respective strong EUV resonance lines, for which direct excitation dominates. All models in the figure are calculated at a single temperature, $T_e = 6$ MK, and the same density, $N_e = 10^{10}$ cm^{-3}, except for SPEX, which is available at the low-density limit.

Most striking is the discrepancy between the EUV and X-ray lines: the observed X-ray fluxes are stronger than predicted fluxes in all models. Even the X-ray $3d$–$2p$ resonance lines, Fe XVIII λ14.208 and Fe XIX λ13.518, are underpredicted relative to their EUV counterparts by more than 30% and a factor of 2, respectively. Since these factors are larger than expected from calibration errors or line blending, it is possible that the accuracy of the direct excitation rate coefficients might explain the predicted weakness of λ14.208 (see Brown et al. 2005); however, it is difficult to reconcile that with the larger discrepancy for λ13.518.

The Fe XVIII and Fe XIX FUV forbidden-line fluxes are in good agreement with the EUV line fluxes of λ93.92 and λ108.37 for the APEC models, and somewhat better than for the FAC rates. FAC does not calculate proton-impact excitation rates, which are included in both APEC and CHIANTI. In APEC models, proton-impact excitation increases the forbidden-line emissivities by 15% and 8% for λ974.86 and λ1118.07, respectively. The predicted FUV line fluxes also begin to increase with density above $N_e \sim 10^{12}$ cm^{-3}. APEC models give the best agreement at $N_e = 2 \times 10^{12}$ cm^{-3} but are also consistent within observational errors with the lower coronal density range.

Figure 1 also shows some large discrepancies among the strongest X-ray lines, reflecting the $3s$–$2p$/$3d$–$2p$ pattern. For these transitions, the largest difference among the predictions results from the number of processes calculated with each model. For example, even though APEC and CHIANTI have similar collision strengths for the Fe XVIII λ15.625 line, additional line flux in APEC is produced by direct excitation to $n = 4$ and $n = 5$ levels, followed by radiative cascades, while CHIANTI currently includes levels only up to $n = 3$. On the other hand, for Fe XVIII λ16.07 APEC and CHIANTI both show differences of more than a factor of 2 from FAC because neither includes the effects of DR on the upper level population, which are included in FAC.

Comparisons of APEC and FAC predictions with the

[6] APEC v1.3 models, calculated at the low-density limit ($N_e = 1.0$ cm^{-3}), and the atomic rate data used to produce them are available at http://cxc.harvard.edu/atomdb. Higher density models are available upon request.

TABLE 1
Fe XVIII AND Fe XIX LINE MEASUREMENTS

Instrument	Ion	λ_{ref} (Å)	λ_{obs} (Å)	Transition	J_U–J_L	Model Flux[a] (photons cm^{-2} ks^{-1})	Observed Flux (photons cm^{-2} ks^{-1})
FUSE[b]	Fe XVIII	974.86	974.85	$2p^5\ ^2P_{1/2}$–$2p^5\ ^2P_{3/2}$	$\frac{1}{2}$–$\frac{3}{2}$	5.063	5.50 ± 0.03
LETG	Fe XVIII	103.93	103.98	$2s2p^6\ ^2S_{1/2}$–$2p^5\ ^2P_{1/2}$	$\frac{1}{2}$–$\frac{1}{2}$	1.625	1.69 ± 0.05
LETG	Fe XVIII	93.923	94.02	$2s2p^6\ ^2S_{1/2}$–$2p^5\ ^2P_{3/2}$	$\frac{1}{2}$–$\frac{3}{2}$	4.441	4.44 ± 0.03
MEG	Fe XVIII	17.623	17.620	$2p^4 3p\ ^2P_{3/2}$–$2s2p^6\ ^2S_{1/2}$	$\frac{3}{2}$–$\frac{1}{2}$	0.300	0.30 ± 0.01
MEG	Fe XVIII	16.159	16.163	$2s2p^5 3s\ ^2P_{3/2}$–$2s2p^6\ ^2S_{1/2}$	$\frac{3}{2}$–$\frac{1}{2}$	0.164	0.13 ± 0.00
MEG[c]	Fe XVIII	16.071	16.073	$2p^4(^3P)3s\ ^4P_{5/2}$–$2p^5\ ^2P_{3/2}$	$\frac{5}{2}$–$\frac{3}{2}$	0.418	0.82 ± 0.01
HEG[c]	Fe XVIII	16.071	16.076	$2p^4(^3P)3s\ ^4P_{5/2}$–$2p^5\ ^2P_{3/2}$	$\frac{5}{2}$–$\frac{3}{2}$	0.418	1.00 ± 0.06
HEG	Fe XVIII[d]	16.004	16.008	$2p^4(^3P)3s\ ^2P_{3/2}$–$2p^5\ ^2P_{3/2}$	$\frac{3}{2}$–$\frac{3}{2}$	0.768	0.81 ± 0.04
HEG	Fe XVIII	15.870	15.873	$2p^4(^1D)3s\ ^2D_{3/2}$–$2p^5\ ^2P_{1/2}$	$\frac{3}{2}$–$\frac{1}{2}$	0.095	0.34 ± 0.02
HEG	Fe XVIII	15.824	15.831	$2p^4(^3P)3s\ ^4P_{3/2}$–$2p^5\ ^2P_{3/2}$	$\frac{3}{2}$–$\frac{3}{2}$	0.179	0.29 ± 0.02
HEG	Fe XVIII	15.625	15.628	$2p^4(^1D)3s\ ^2D_{5/2}$–$2p^5\ ^2P_{3/2}$	$\frac{5}{2}$–$\frac{3}{2}$	0.290	0.43 ± 0.02
HEG	Fe XVIII	14.571	14.559	$2p^4(^3P)3d\ ^4P_{3/2}$–$2p^5\ ^2P_{3/2}$	$\frac{3}{2}$–$\frac{3}{2}$	0.110	0.21 ± 0.07
HEG	Fe XVIII	14.534	14.539	$2p^4(^3P)3d\ ^2F_{5/2}$–$2p^5\ ^2P_{3/2}$	$\frac{5}{2}$–$\frac{3}{2}$	0.210	0.39 ± 0.09
HEG	Fe XVIII	14.373	14.376	$2p^4(^3P)3d\ ^2D_{5/2}$–$2p^5\ ^2P_{3/2}$	$\frac{5}{2}$–$\frac{3}{2}$	0.278	0.55 ± 0.02
HEG	Fe XVIII[e]	14.256	14.261	$2p^4(^1D)3d\ ^2S_{1/2}$–$2p^5\ ^2P_{3/2}$	$\frac{1}{2}$–$\frac{3}{2}$	0.087	0.42 ± 0.03
…	…	…	…	$2p_{1/2}2p^3_{3/2}3d_{5/2}$–$2p^5\ ^2P_{3/2}$	$\frac{5}{2}$–$\frac{3}{2}$	0.141	…
HEG	Fe XVIII	14.208	14.208	$2p_{1/2}2p^3_{3/2}3d_{5/2}$–$2p^5\ ^2P_{3/2}$	$\frac{3}{2}$–$\frac{3}{2}$	0.381	1.40 ± 0.05
…	…	…	…	$2p^4(^1D)3d\ ^2D_{5/2}$–$2p^5\ ^2P_{3/2}$	$\frac{5}{2}$–$\frac{3}{2}$	0.695	…
HEG	Fe XVIII	11.527	11.528	$2p^2_{1/2}2p^2_{3/2}4d_{5/2}$–$2p^5\ ^2P_{3/2}$	$\frac{5}{2}$–$\frac{3}{2}$	0.032	0.17 ± 0.01
…	…	…	…	$2p^4(^3P)4d\ ^2D_{5/2}$–$2p^5\ ^2P_{3/2}$	$\frac{5}{2}$–$\frac{3}{2}$	0.061	…
HEG	Fe XVIII	11.423	11.424	$2p^4(^3P)4d\ ^2F_{5/2}$–$2p^5\ ^2P_{3/2}$	$\frac{5}{2}$–$\frac{3}{2}$	0.080	0.13 ± 0.01
…	Fe XXII	11.427	…	$2s2p_{1/2}3p_{3/2}$–$2p\ ^2P_{1/2}$	$\frac{3}{2}$–$\frac{1}{2}$	0.007	…
HEG	Fe XVIII	11.326	11.327	$2p^4(^1D)4d\ ^2S_{1/2}$–$2p^5\ ^2P_{3/2}$	$\frac{1}{2}$–$\frac{3}{2}$	0.019	0.13 ± 0.02
…	…	…	…	$2p^4(^1D)4d\ ^2P_{3/2}$–$2p^5\ ^2P_{3/2}$	$\frac{3}{2}$–$\frac{3}{2}$	0.031	…
…	…	…	…	$2p^4(^1D)4d\ ^2D_{5/2}$–$2p^5\ ^2P_{3/2}$	$\frac{5}{2}$–$\frac{3}{2}$	0.038	…
FUSE	Fe XIX[b,f]	1118.07	…	$2p^4\ ^3P_1$–$2p^4\ ^3P_2$	1–2	1.833	1.74 ± 0.22
LETG	Fe XIX	120.00	120.04	$2s2p^5\ ^3P_2$–$2p^4\ ^3P_1$	2–1	0.836	0.97 ± 0.03
LETG	Fe XIX	111.70	111.74	$2s2p^5\ ^3P_1$–$2p^4\ ^3P_1$	1–1	0.326	0.46 ± 0.02
LETG	Fe XIX	109.97	109.99	$2s2p^5\ ^3P_1$–$2p^4\ ^3P_0$	1–0	0.413	0.46 ± 0.02
LETG	Fe XIX	108.37	108.39	$2s2p^5\ ^3P_2$–$2p^4\ ^3P_2$	2–2	3.091	3.13 ± 0.05
LETG	Fe XIX	101.55	101.59	$2s2p^5\ ^3P_1$–$2p^4\ ^3P_2$	1–2	0.838	1.02 ± 0.03
LETG	Fe XIX	91.02	91.054	$2s2p^5\ ^1P_1$–$2p^4\ ^1D_2$	1–2	0.241	0.45 ± 0.02
HEG	Fe XIX	16.110	16.111	$2p_{1/2}2p^2_{3/2}3p_{1/2}$–$2s2p^5\ ^3P_2$	2–2	0.120	0.14 ± 0.03
HEG	Fe XIX	15.198	15.204	$2p^2_{1/2}2p^2_{3/2}3s$–$2s2p^5\ ^3P_2$	2–2	0.080	0.39 ± 0.02
HEG	Fe XIX	15.079	15.083	$2p^3(^4S)3s\ ^5S_2$–$2p^4\ ^3P_2$	2–2	0.094	0.33 ± 0.02
HEG	Fe XIX	14.664	14.671	$2p^3(^2D)3s\ ^3D_3$–$2p^4\ ^3P_2$	3–2	0.079	0.21 ± 0.01
HEG	Fe XIX	13.795	13.795	$2p_{1/2}2p^2_{3/2}3d_{5/2}$–$2p^4\ ^3P_2$	3–2	0.105	0.24 ± 0.02
…	…	…	…	$2p^3(^2D)3d\ ^3P_2$–$2p^4\ ^3P_2$	3–2	0.012	…
HEG	Fe XIX	13.518	13.523	$2p^3(^2D)3d\ ^3D_3$–$2p^4\ ^3P_2$	3–2	0.262	0.52 ± 0.03
HEG	Fe XIX	13.497	13.507	$2p_{1/2}2p^2_{3/2}3d_{3/2}$–$2p^4\ ^3P_2$	2–2	0.118	0.32 ± 0.02
…	Fe XXI	13.507	13.507	$1s^2 2s2p^2_{1/2}3s$–$1s^2 2s2p^3\ ^3D_1$	2–2	0.025	…
HEG	Fe XIX	13.462	13.470	$2p^3(^2D)3d\ ^3S_1$–$2p^4\ ^3P_2$	1–2	0.072	0.25 ± 0.02
HEG	Ne IX	13.447	13.446	$1s^2\ ^1S_0$–$1s2p\ ^1P_1$	1–2	0.397	0.40 ± 0.02

[a] Line blends are listed separately if they contribute more than 10% to the Fe line of interest (in the model). Fluxes (including blends) normalized to the λ93.92 line predicted by the EMD model using APEC at a density of 1 cm^{-3} are listed. The observed fluxes have been corrected for interstellar absorption using $N_H = 1.7 \times 10^{18}$ cm^{-2} (Piskunov et al. 1997), neutral helium, and H/He abundance ratio set at 11.6 (Kimble et al. 1993). The largest correction at λ120.0 amounts to only 9%.

[b] See Young et al. 2001.

[c] MEG and HEG measurements of this line are given to show the cross-calibration. HEG is preferred for this analysis because of its better spectral resolution.

[d] Contribution of O VIII to this line is more than 50%.

[e] LETG flux was measured to cross-check the calibration of LETG vs. HETG. The LETG line is somewhat blended, but the flux is within 30% of the HETG flux.

[f] This *FUSE* measurement is uncertain, as this line is blended. Solar-network spectra were used to estimate the contribution of C I to the blend.

observed fluxes of the X-ray lines listed in Table 1 are shown in Figure 2. We confirm a general $3s$–$2p$/$3d$–$2p$ discrepancy pattern for APEC models that is largely removed with the FAC calculations. The $3s$–$2p$/$3d$–$2p$ ratios of the summed line fluxes from APEC are smaller than the observed ratios by ∼20%, whereas FAC agreement is within 10%. The inclusion of DR in the FAC models produces the additional $3s$–$2p$ line emissivity.

Another significant disagreement between the models and observations occurs for radiative transitions that terminate on excited levels, namely, Fe XVIII λ15.870, λ16.159, and λ17.623 and Fe XIX λ15.198 and λ16.110. Although the APEC line list, which is reasonably complete in this spectral region, does not include DR satellite lines from either Fe XVIII or Fe XIX, blending with satellite lines or lines from other ions cannot explain the extent of the underprediction. It is possible that the large theoretical wavelength inaccuracies for these lines, up to a few

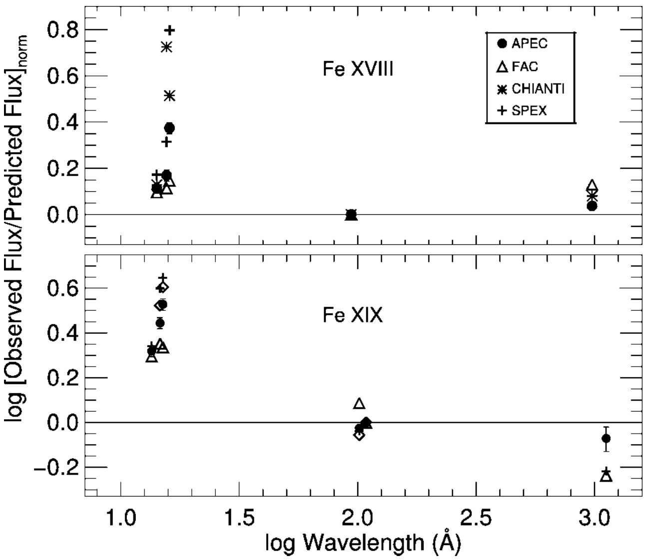

FIG. 1.—The observed-to-predicted flux ratios of strong lines in the X-ray, EUV, and FUV spectral regions. Shown for comparison are the ratios obtained using the APEC, CHIANTI, and SPEX spectral codes and the FAC rates. The density is $N_e = 10^{10}$ cm^{-3}, except for SPEX. *Top*: Comparison for Fe XVIII lines, normalized to λ93.92. The X-ray lines plotted here are λ14.208, λ15.625, and λ16.071. *Bottom*: Comparison for Fe XIX lines, normalized to λ108.37. The X-ray lines plotted are λ13.518, λ14.664, and λ15.079.

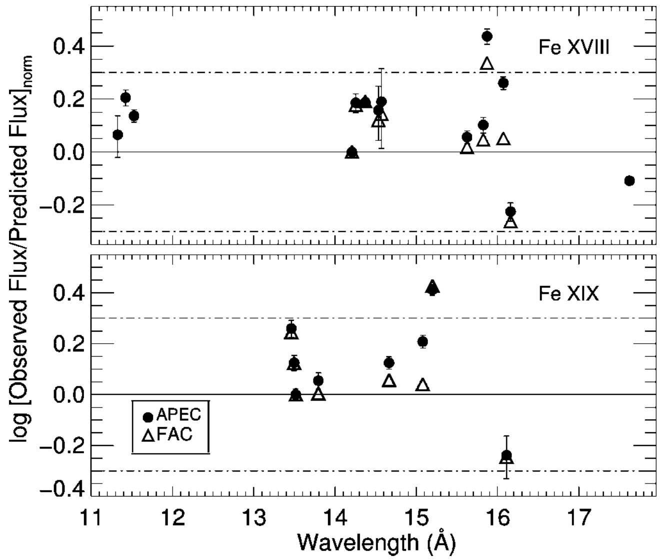

FIG. 2.—The observed-to-predicted flux ratios of X-ray lines using FAC and APEC. Lines from Table 1 excluding heavily blended Fe XVIII λ16.004 are shown. Note the 3*d*–2*p* lines are between 14 and 15 Å for Fe XVIII and shortward of 14 Å for Fe XIX. Ratios are calculated at $N_e = 10^{10}$ cm^{-3}. Dash-dotted lines represent agreement within a factor of 2. *Top*: Comparison for Fe XVIII, normalized to λ14.208. There are no published FAC models for Fe XVIII 4*d*–2*p* lines around 11.4 Å. *Bottom*: Comparison for Fe XIX, normalized to λ13.518.

percent, have led to misidentifications in the laboratory measurements. Blending of nearby lines from the same ion could produce such a pattern of under- and overprediction. For Fe XVIII λ15.870, this latter explanation is consistent with new wavelength calculations (Kotochigova et al. 2005; Gu 2005).

4. CONCLUSIONS

A surprising result of this benchmark spectral modeling study is the large discrepancy between modern theory and the Capella observations for the X-ray and EUV resonance lines of Fe XVIII (30%) and Fe XIX (factor of 2). New FAC calculations including dielectronic recombination bring most X-ray lines into good agreement with observations; however, puzzling discrepancies as large as a factor of 2 still remain for some relatively strong lines. Additional laboratory and theoretical work is needed to eliminate the largest remaining problems. Meanwhile, errors can largely be minimized by judicious choice of line diagnostics and consideration of appropriate atomic processes.

This work is supported in part by the *Chandra* X-Ray Center (NAS 8-39073). We thank the CXC staff, particularly Harvey Tananbaum, for supporting efforts to obtain these data, and the developers of the other public spectral modeling codes SPEX and CHIANTI, as well as M.-F. Gu for the atomic structure code FAC.

REFERENCES

Anders, E., & Grevesse, N. 1989, Geochim. Cosmochim. Acta, 53, 197
Beiersdorfer, P., et al. 2002, ApJ, 576, L169
Berrington, K. A., Saraph, H. E., & Tully, J. A. 1998, A&AS, 129, 161
Brickhouse, N. S., & Drake, J. 2000, Rev. Mex. AA Ser. Conf., 9, 24
Brickhouse, N. S., Dupree, A. K., Edgar, R. J., Liedahl, D. A., Drake, S. A., White, N. E., & Singh, K. P. 2000, ApJ, 530, 387
Brickhouse, N. S., Raymond, J. C., & Smith, B. W. 1995, ApJS, 97, 551
Brinkman, A. C., et al. 2001, A&A, 365, L324
Brown, G. V., Beiersdorfer, P., Liedahl, D. A., Widmann, K., & Kahn, S. M. 1998, ApJ, 502, 1015 (erratum 532, 1245 [2000])
Brown, G. V., Beiersdorfer, P., Liedahl, D. A., Widmann, K., Kahn, S. M., & Clothiaux, E. J. 2002, ApJS, 140, 589
Brown, G. V., et al. 2005, in AIP Conf. Proc., X-Ray Diagnostics for Astrophysical Plasmas, ed. R. K. Smith (New York: AIP), in press
Canizares, C. R., et al. 2000, ApJ, 539, L41
Cash, W. 1979, ApJ, 228, 939
Dere, K. P., Landi, E., Mason, H. E., Monsignori Fossi, B. C., & Young, P. R. 1997, A&AS, 125, 149
Foster, V. J., Keenan, F. P., & Reid, R. H. J. 1994, At. Data Nucl. Data Tables, 58, 227
Freeman, P., Doe, S., & Siemiginowska, A. 2001, Proc. SPIE, 4477, 76
Gu, M.-F. 2003, ApJ, 582, 1241
———. 2005, ApJS, 156, 105
Kaastra, J. S., Mewe, R., & Nieuwenhuijzen, H. 1996, in Proc. 11th Conference on UV and X-Ray Spectroscopy of Laboratory and Astrophysical Plasmas, ed K. Yamashita & T. Watanabe (Tokyo: Univ. Acad. Press), 411
Kimble, R. A., Davidsen, A. F., Long, K. S., & Feldman, P. D. 1993, ApJ, 408, L41
Kotochigova, S., Kirby, K. P., Brickhouse, N. S., Mohr, P. J., & Tupitsyn, I. I. 2005, in AIP Conf. Proc., X-Ray Diagnostics for Astrophysical Plasmas, ed. R. K. Smith (New York: AIP), in press
Laming, J. M., et al. 2000, ApJ, 545, L161
Liedahl, D. A., Osterheld, A. L., & Goldstein, W. H. 1995, ApJ, 438, L115
Mewe, R., Kaastra, J. S., & Liedahl, D. A. 1995, Legacy, 6, 16
Piskunov, N., Wood, B. E., Linsky, J. L., Dempsey, R. C., & Ayres, T. R. 1997, ApJ, 474, 315
Saba, J. L. R., Schmelz, J. T., Bhatia, A. K., & Strong, K. T. 1999, ApJ, 510, 1064
Safronova, U. I., Vasilyev, A. A., & Smith, R. K. 2001, Canadian J. Phys., 78, 1055
Smith, R. K., Brickhouse, N. S., Liedahl, D. A., & Raymond, J. C. 2001, ApJ, 556, L91
Xu, H., et al. 2002, ApJ, 579, 600
Young, P. R., Del Zanna, G., Landi, E., Dere, K. P., Mason, H. E., & Landini, M. 2003, ApJS, 144, 135
Young, P. R., Dupree, A. K., Wood, B. E., Redfield, S., Linsky, J. L., Ake, T. B., & Moos, H. W. 2001, ApJ, 555, L121